# *Analytical Solutions for Steady Phreatic Flow Appearing/Re-emerging Toward/ from a Bedrock/Caprock Isobaric Breach: The Polubarinova-Kochina–Numerov and Pavlovsky Problems Revisited*

**Yu. V. Obnosov, A. R. Kacimov & O. Castro-Orgaz**

**Transport in Porous Media**

ISSN 0169-3913

Transp Porous Med
DOI 10.1007/s11242-015-0522-9

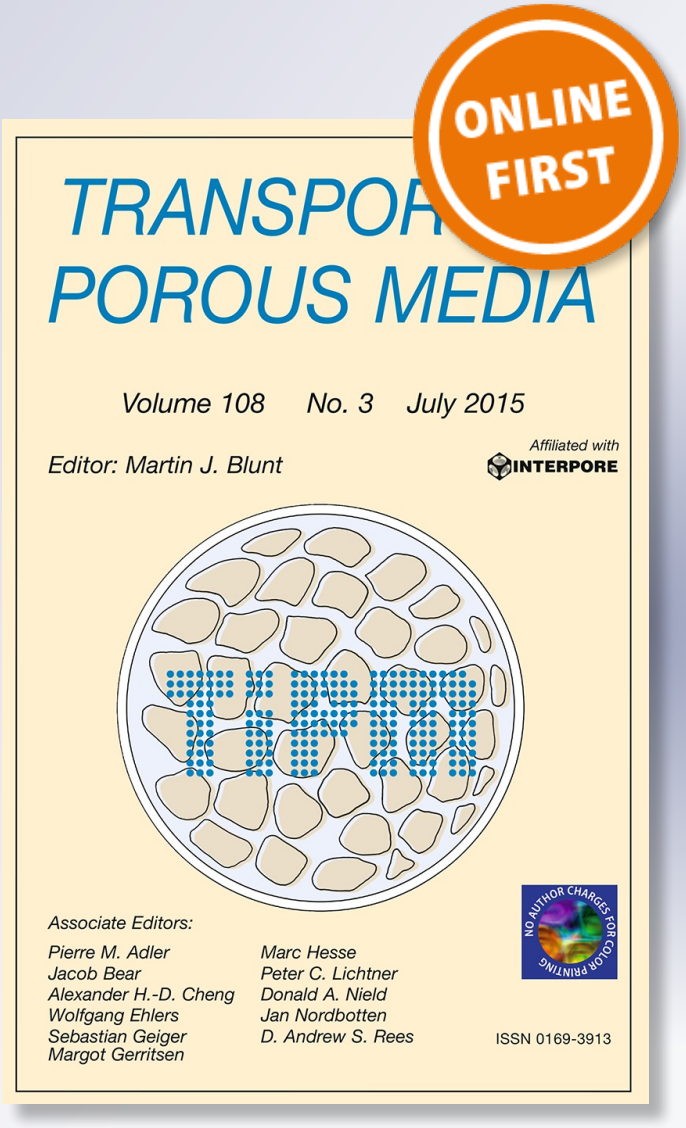


Springer

Transp Porous Med
DOI 10.1007/s11242-015-0522-9

# Analytical Solutions for Steady Phreatic Flow Appearing/Re-emerging Toward/from a Bedrock/Caprock Isobaric Breach: The Polubarinova-Kochina–Numerov and Pavlovsky Problems Revisited

**Yu. V. Obnosov**[1] · **A. R. Kacimov**[2] · **O. Castro-Orgaz**[3]

Received: 6 March 2015 / Accepted: 22 May 2015


**Abstract** Analytical solutions for steady, confined and unconfined Darcian flows in aquifers breached by "windows" in caprocks or bedrocks with applications to hillslope hydrology are presented. As compared with classical Polubarinova-Kochina, Numerov and Pavlovsky analytical solutions, the aquifers are sloping and the "window" is a finite-size isobaric segment, which due to the aquifer dip brings about a nonconstant head boundary condition. The velocity hodograph, method of boundary value problems and conformal mappings are used for obtaining solutions of essentially 2D seepage problems with Laplace's PDE as a governing equation and the nonlinear phreatic surface for an unconfined flow. The second-order hydraulic theory with Picard's iteration is used for deriving and solving a nonlinear ODE with respect to the shape of the water table, that is, compared with standard Dupuit–Forchheimer computations. The size of the "window," incident flow parameters upstream of the "window" and the angle of tilt determine the disturbance to a main aquifer, mundanely normal "longitudinal" flow, which may completely dive or unexpectedly extravasate into a commingled adjacent subjacent–superjacent layer.

**Keywords** Sloping aquifer · Complex potential · Darcian velocity · DF approximation · Hydraulic theory

✉ Yu. V. Obnosov
yobnosov@kpfu.ru

A. R. Kacimov
anvar@squ.edu.om; akacimov@gmail.com

O. Castro-Orgaz
oscarcastro@ias.csic.es; ag2caoro@uco.es

[1] Institute of Mathematics and Mechanics, Kazan Federal University, Kazan, Russia

[2] Department of Soils, Water and Agricultural Engineering, Sultan Qaboos University, Muscat, Oman

[3] University of Cordoba, Spain, Campus Rabanales, Leonardo Da Vinci Building, Madrid Road km 396, 14071 Córdoba, Spain

Published online: 06 June 2015

## Abbreviations

| | |
|---|---|
| BVP | Boundary value problem |
| DF | Dupuit–Forchheimer |
| PK | Polubarinova-Kochina [reference to Polubarinova-Kochina (1977)] |

*I'm going to emerge then submerge.*
*George W. Bush*

## 1 Introduction

Hydrogeologist, soil pedologists and reservoir engineers have recently recognized that the old paradigm of layered aquifers, soil horizons and pays, derived from basic sedimentology, often fails to explain the dynamics of fluids in commingled formations. Field distributions of hydraulic heads, water table elevations, pore pressures, Darcian velocities, phase saturations, ground-quality, soil-quality, water-quality tracer tests, among others, exhibit anomalies (e.g., sudden blips in the phreatic surface elevation), which cannot be explained by standard PEST-MODFLOW massaging of hydraulic or geometrical characteristics of the posited layers.

In the "layer" paradigm, flow/transport is viewed as either 1D or quasi-1D. For example, in classical groundwater hydrology, flow in a multilayered system of highly permeable alluvial aquifers with sandwiched low-permeable aquitardsis "decoupled": Strata of high/low permeability are considered as zones where flow is along/across the formation, correspondingly, with the so-called exchange (leakage) 1D fluxes between the highly conductive layers (see, e.g., Hemker 1984). Aquicludes (formations of extremely low permeability) are modeled as impervious bedrocks/ caprocks. Similarly, in standard oil reservoir management, shale layers are conceptualized as an impermeable partitioning between the pays. Groundwater–oil engineers, driven by a pragmatic interest to "pump out" a fluid, benchmarked flows in layered systems against the seminal Theis model of 1D radial flow toward a vertical well, with a Hantush-type leakage. In soil physics, pedon-evidenced ideal layering led to conceptualization of 1D vertical saturated and saturated-unsaturated flows, with gravity and capillarity playing a crucial role. Flow models of Green-Ampt and Philip were, again, aligned with a practical motivation to describe rainfall- and irrigation-induced infiltration.

The real hydrostratigraphy in hydrogeology and pedogenesis occurred to be much more complicated: The bedrocks–caprocks and interfaces between the soil horizons are not straight (flat), hydraulic properties of porous massifs vary both "longitudinally" and "transversally" with respect to the expected dominating flow-transport directions, and various hydraulic encumbrances impede otherwise 1D flow, among others. This becomes especially important in regional scale groundwater models (see, e.g., Toth 2009) and in hillslope hydrology (see, e.g., Broda et al. 2011; Dusek and Vogel 2014; Gabrielli et al. 2012; George and Conacher 1993; Hardie et al. 2012; Harte and Winter 1995; Iwagami et al. 2010; Kacimov 2012; Kacimov et al. 2015; Read and Volker 1993; Tromp-van Meerveld et al. 2007; Wang et al. 2014), where the effect of gravity on flow topology and chemicals' spread is intricately intertwined with aquifers–aquitards–aquicludes heterogeneity, geometry of boundaries between hydrostratigraphic units and boundary conditions (e.g., constant head versus constant pressure) at the inlets–outlets of composite groundwater or soilwater "flow tubes."

In this paper we use the language of groundwater hydrology and present explicit analytical solutions for steady, Darcian, unconfined and confined flows in an aquifer commingled with a subjacent or superjacent layer via a finite-size "window" or "conduit" of much higher perme-

ability. This "window" represents faults in structural geology. Bense et al. (2013) noticed the deficit of hydrogeological models, capable to describe flow in the vicinity of faults. Along with faults, karst caves, highly fractured aquifer beds or man-made rock openings in shale (the so-called fracking revolution, see, e.g., Gassiat et al. 2013) alter otherwise simple 1D flows and make them inherently 2D or 3D. This calls for advanced mathematical techniques such as the method of hodograph, Hilbert and Riemann boundary value problems and the Polubarinova-Kochina (1977, hereafter abbreviated as PK) method of linear differential equations.

PK presented analytical solutions for unconfined groundwater flows in homogeneous soils over bedrocks inclined at a constant slope. She considered a phreatic surface of a "normal" 1D flow parallel to an impermeable bedrock disturbed by seepage from a zero-depth channel or toward a Zhukovsky drain (her book pages 74–76, 233–239). The resulting 2D phreatic flow from/to the channel/drain, which either supplements the incident flow or partially depletes it, is topologically complex, similar to the confined losing–gaining–flow-through lakes of Townley and Trefry (2000) and Kacimov (2007). PK used a 2D potential model and theory of holomorphic functions for the analysis of the emerging multiple-connected and even nonmonotonic phreatic surfaces. Another subsurface system addressed by PK in studies of sloping unconfined aquifers involved a substratum of hydraulic conductivity contrasting with that of the upper aquifer (her book, pages 389–390). In solving this problem for a composite commingled aquifer, PK utilized the hydraulic theory, i.e., the Dupuit–Forchheimer's (DF) approximation. The classical DF hydraulic theory as presented in PK is of first order, that is, a hydrostatic pressure distribution is assumed across the saturated thickness. This theory can be expanded to any order of accuracy by iteration of the Cauchy–Riemann conditions using Picard's method (Castro-Orgaz et al. 2012; Castro-Orgaz and Hager 2014; Kacimov et al. 2015).

In this paper we extend the PK analysis. We consider a hillslope consisting of two hydrostratigraphic units: a highly permeable upper layer of hydraulic conductivity $k_1$ and a subjacent low-permeable layer of conductivity $K_2$ (Fig. 1 represents a vertical cross section). The second layer is bounded from below by a third layer (aquifuge) of almost zero conductivity $K_3$ such that $k_1 \gg K_2 \gg K_3$. Somewhere upstream the upper layer is naturally recharged during rainfalls such that an unconfined steady-state flow of a saturated thickness $B$ is formed in the upper aquifer. Downstream in the valley, layers 1 and 2 are discharged into a river (wadi channel) as base flow. The roots of hillslope vegetation are hydroecologically gaining from the first layer as schematically depicted in Fig. 1. Bense et al. (2013) attributed distinct ecotones of natural plants to sudden fault-caused drops of the water table.

We consider both layers in Fig. 1 having zones of a low hydraulic conductivity, $\lambda_1 \ll K_2$, and high conductivity, $k_2 \ll k_1$, demarcated in Fig. 1 by dash-dotted segments. Consequently, permeability in Fig. 1 varies longitudinally, along the prevailing flow direction from the mountain recharge zone to the valley, and transversally. As result of this heterogeneity, flow "dives" from the upper aquifer into the second one through a "window" GF of width $R_F$ and re-emerges from the second aquifer back to the first one through a "window" AC of a width $r$. The part of the upper aquifer above $\mathrm{NFB}_2 A_t$ remains dry. As Fig. 1 depicts, the topology of flow, caused by interaction of the adjacent aquifers, and groundwater quality, which depends on residence time within each porous compartment of Fig. 1, become intricately nontrivial. Two zones of Fig. 1, an unconfined aquifer 1, drained by the "window" GF and a confined aquifer 2, with a vent through the "window" AC, are zoomed in Figs. 2 and 5, respectively. It is noteworthy that groundwater flows like one in Fig. 1 and Kacimov and Brown (2015) have been recently modeled in reconstruction of paleogroundwater hydrology of Mars (Marra et al. 2014) where the gravity constant $g$ is different from Earth.

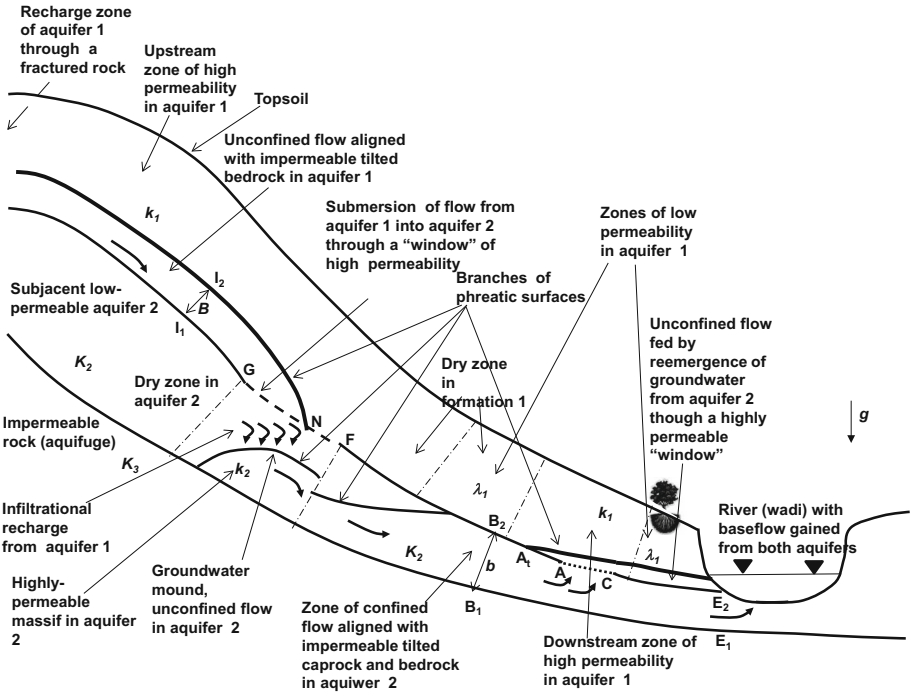


**Fig. 1** Vertical cross section of two aquifers, commingled through two "windows"

## 2 Confined Flow with Losses to a Seepage Face in Caprock

In this section we study an analytic element (see Strack 1989 on the method of analytic elements) near the "window" $AC$ in Fig. 1 where Bush's re-emergence (see the epigraph) of groundwater from a subjacent confined aquifer takes place. In terms of Marra et al. (2014) this is a "pressurized groundwater release." Modeling of "windows" of a constant hydraulic head and topological analysis of the gaining, losing and flow-through regimes in confined aquifers without tilt has been carried by Aravin and Numerov (1953, see their Fig. 99, Ch. 5, Section 52). Similarly, PK-77 (see her Fig. 141, Ch. VI, Section 1) analyzed injection of groundwater into a "window" of a constant recharge rate. In this paper we add to this analysis two extra factors: the dipping nature of an aquifer and gravity, which is involved through an isobaric (seepage face) condition along the "window" boundary.

The incident flow rate $Q$ is partially intercepted by exfiltration through a caprock breach, with $k_1 \gg K_2 \gg \lambda_1$. Downstream of the breach the flow rate drops to $0 < q < Q$. We zoom the flow zone close to $AC$ in Fig. 1 as Fig. 2a where we assume that the thickness $b$ and the slope $\alpha\pi$, $\alpha < 1/2$ are constant.

We introduce Cartesian coordinates $xAy$, with the origin $A$ coinciding with the upper edge of the breach (Fig. 2a). The bedrock $B_1E_1$ is an impermeable line tilted at an angle $\alpha\,\pi$, $0 < \alpha < 1/2$ with respect to the abscissa axis. The caprock $B_2E_2$ is parallel to $B_1E_1$ but consists of three segments: The rays $AB_2$ and $CE_2$ are also impermeable but the segment $AC$ (the breach) is an isobaric line through which the main confined aquifer is in a hydraulic contact with the upper aquifer of a much higher conductivity $k_1 \gg K_2$. Through $AC$ groundwater extravasates into the upper formation where an unconfined "plume" bounded by a phreatic

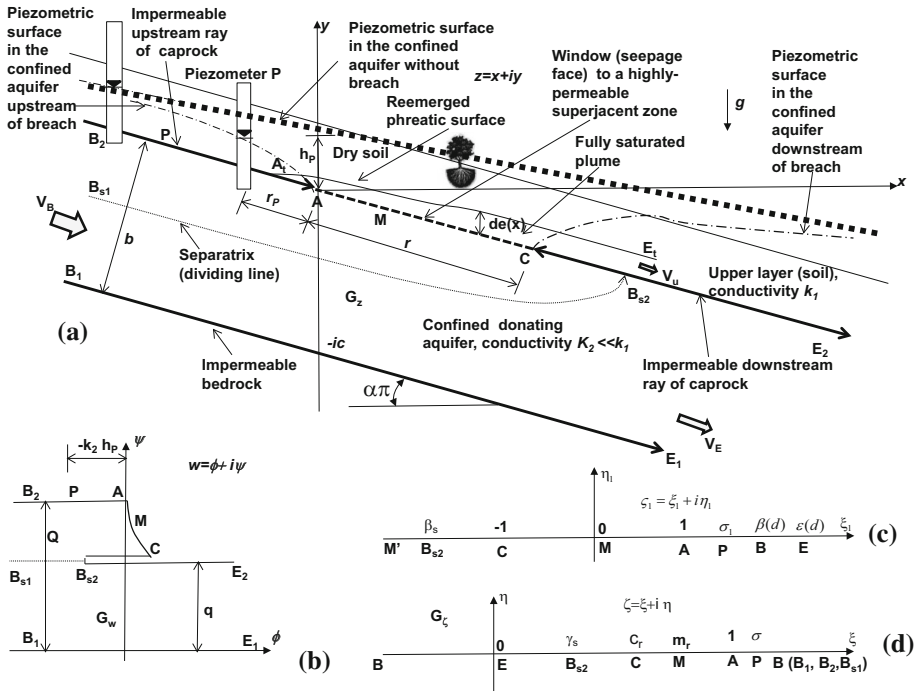


**Fig. 2** Confined aquifer discharging through a caprock window: physical flow domain (**a**), complex potential domain (**b**), two auxiliary planes (**c**, **d**)

surface $A_t P_2$ is formed. This plume has a variable thickness de($x$). We assume that the donated quantity $Q - q$ is small enough (i.e., $r$ is small enough). Therefore, de($x$) is relatively small and along $A_t C$ pressure is almost atmospheric. There is a small "upwelling" tip, $AA_t$, of the phreatic surface in the first aquifer, which will be here ignored.

The curve $B_{s1}B_{s2}$ in Fig. 2a is a separatrix: It divides the incident flow in the main aquifer into a part out-seeping into the upper aquifer and a part which continues its confined journey to point E. The point $B_{s2}$ is a stagnation (bifurcation) point. Similar to Kacimov (2007) and Townley and Trefry (2000), other topological regimes are possible. For example, for large $r$ $B_{s2}$ is located between points $A$ and $C$, i.e., the breach $AC$ is partially exfiltrating and partially infiltrating, in terms of the Toth (2009) model, in which a "seepage face" ground surface on a catchment scale is a distributed sink source with respect to the fully saturated subsurface. The value of $q$ can be negative if the breach is close to the downstream discharge segment $E_2E_1$ in Fig. 1 and the head in the tailwater reservoir commands over the breach: In this case water moves to AC both from the right and left in Fig. 2a. These "exotic" regimes will not be addressed in this paper.

We introduce the hydraulic head $h(x, y)$ which is a harmonic function in the flow domain $G_z$ (a tilted strip of the lower aquifer in Fig. 2a). We introduce a complex potential $w = \varphi + i\psi$, where $\varphi = -K_2 h$ is the velocity potential and $\psi$ is a stream function.

As we assumed that $AC$ is a zero gauge pressure line, we count the head from a fiducial point $A$ where $\phi = 0$, $\psi = Q$ and stream function—from $B_1E_1$, along which, $\psi = 0$. The value of $Q$ is known but the value of $q$ is not. At point $P$ a piezometer is installed and the hydraulic head there is measured as $h = h_P > 0$. The distance from $A$ to $P$ along the

caprock is $r_P$. Far from the breach the piezometric line (Fig. 2a, dash-dotted line) is an almost straight line, i.e., far upstream and downstream of the breach flow is 1D. Close to the breach this line curves. Along the breach the peizometric line coincides with the breach boundary (dashed line in Fig. 2a). Near point $B_{s2}$ the piezometric curve has a local maximum. If $r = 0$ (no breach) the piezometric surface is a straight line (bold-dotted in Fig. 2a).

Along AC $\varphi + K_2 y = 0$. The complex velocity, $V(x, y)$, is an antiholomorfic function $V = \overline{\mathrm{d}w/\mathrm{d}z}$ where the overbar stands for complex conjugation. Then, at point $B$ upstream of the window $|V| = V_B = Q/b$. Similarly, at point $E$ downstream $|V| = V_E = q/b$. At both points the velocity vector is parallel to the bedrock and caprock rays.

The complex potential domain $G_w$ is shown in Fig. 2b. Here, the image of $AC$ is an unknown curve. There is a cut $CB_{s2}E_2$ in $G_w$.

Our main goal is to determine how $q$ depends on aquifer's geometrical characteristics: $\alpha, b$ and the breach size $r$ (Fig. 2a), the parameters of the incident flow, $Q, h_P, r_P$ and conductivity $K_2$.

We map conformally the strip $G_z$ onto an auxiliary half plane $\zeta > 0$, $\varsigma = \xi + i\,\eta$ in Fig. 2c with the correspondence of points $E \to 0$, $A \to 1$, $B \to \infty$

$$z(\varsigma) = \frac{b}{\pi}\, e^{i\pi(1-\alpha)} \log \varsigma. \tag{1}$$

Then, point C is imaged as $C \to c_r = e^{-\pi r/b}$. Similarly, for the piezometer point $P \to \sigma = e^{\pi r_P/b}$ and for the stagnation point $B_{s2} \to \beta_s$. Obviously, at points $A$ and $C$ the Darcian velocity vector $\vec{V}$ and complex velocity function $V$ are infinite. At a certain point $M$ in between $A$ and $C$ the velocity attains a minimum magnitude $V_M$. The affix of point M in the $\zeta$-plane is $m_r$.

We have to solve the following mixed boundary value problem (BVP) for an analytic function $w(\zeta)$:

$$\begin{aligned} B_1E_1 &: \psi = 0, \quad y = -c - x\tan\pi\alpha, \\ E_2C &: \psi = q, \quad y = -x\tan\pi\alpha, \\ CA &: \varphi = -K_2 y(\xi), \quad y = -x\tan\pi\alpha, \\ AB_2 &: \psi = Q, \quad y = -x\tan\pi\alpha, \end{aligned} \tag{2}$$

where $c = b\cos\pi\alpha$ and $y(\xi) = (b/\pi)\sin\pi\alpha\log\xi$ is taken from Eq. (1). It is noteworthy that at points $A$ and $C$ the function $w(\zeta)$ is finite and at points $B$ and $E$ it has the same logarithmic singularity as $z(\zeta)$.

We consider an auxiliary function

$$w_0(\varsigma) = \frac{q}{\pi}\log(-\varsigma) - \frac{Q-q}{\pi}\log\left(m(\varsigma) + \sqrt{m(\varsigma)^2 - 1}\right), \quad m(\varsigma) = \frac{1 + c_r - 2\varsigma}{1 - c_r}. \tag{3}$$

The branch of the first summand in Eq. (3) is fixed in the upper half of the $\varsigma$-plane by the condition $-\pi < \arg(-\varsigma) < 0$. The fixed branch of the second summand in (3) maps conformally the upper half of the $\varsigma$-plane onto the half strip $\{\varsigma : \mathrm{Re}\varsigma < 0, 0 < \mathrm{Im}\varsigma < Q-q\}$. The imaginary part of $w_0(\xi)$ has jumps $-q$ and $-Q$ at the points $\varsigma = 0$ and $\varsigma = \infty$, correspondingly; namely,

$$\begin{aligned} &\mathrm{Im}[w_0(\xi)] = 0, \quad -\infty < \xi < 0; \\ &\mathrm{Im}[w_0(\xi)] = -q, \quad 0 < \xi < c_r; \end{aligned}$$

$$\mathrm{Re}[w_0(\xi)] = q/\pi \log \xi, \quad c_r < \xi < 1;$$
$$\mathrm{Im}[w_0(\xi)] = -Q, \quad 1 < \xi < \infty.$$

Hence, a function $W(\varsigma) = w(\varsigma) + w_0(\xi)$ is holomorphic in the upper half of the $\varsigma$-plane and satisfies the following boundary conditions:

$$\mathrm{Im}W(\xi) = 0, \quad \xi \in (-\infty, c_r) \cup (1, \infty),$$
$$\mathrm{Re}W(\xi) = \frac{q - k_2 b \sin \pi\alpha}{\pi} \log \xi = g(\xi), \quad \xi \in (c_r, 1). \tag{4}$$

It is noteworthy that at points $E$ and $B$ the function $W(\varsigma)$ does not have singularities, although the functions $w(\varsigma)$ and $z(\varsigma)$ do. Similarly, at the transition points $A$ and $C$, i.e., where the boundary conditions (4) change, the behavior of $W(\varsigma)$ is regular.

The solution of problem (4), which is bounded at both transition points $\varsigma = C_r$ and $\varsigma = 1$ as well as at infinity, is represented by the Signorini formula as the following singular integral (see Gakhov 1966):

$$w(\varsigma) = \frac{\sqrt{(\varsigma - c_r)(1 - \varsigma)}}{\pi i} \int_{c_r}^{1} \frac{g(\tau)\, \mathrm{d}\tau}{\sqrt{(\tau - c_r)(1 - \tau)}(\tau - \varsigma)} - w_0(\varsigma), \tag{5}$$

$$w(\varsigma) = \frac{\sqrt{(\varsigma - c_r)(1 - \varsigma)}}{\pi^2 i} \int_{c_r}^{1} \frac{(q - k_2 b \sin \pi\alpha) \log \tau \mathrm{d}\tau}{\sqrt{(\tau - c_r)(1 - \tau)}(\tau - \varsigma)}$$
$$+ \frac{Q - q}{\pi} \log\left(m(\varsigma) + \sqrt{m(\varsigma)^2 - 1}\right) - \frac{q}{\pi} \log(-\varsigma). \tag{6}$$

We transform the integral in Eq. (6) as

$$\frac{1}{\pi i} \int_{c_r}^{1} \frac{\log \tau \mathrm{d}\tau}{\sqrt{(\tau - c_r)(1 - \tau)}(\tau - \varsigma)} = \frac{1}{\pi i} \int_{c_r}^{1} \frac{(\log \tau - \log \varsigma)\, \mathrm{d}\tau}{\sqrt{(\tau - c_r)(1 - \tau)}(\tau - \varsigma)}$$
$$+ \frac{\log \varsigma}{\pi i} \int_{c_r}^{1} \frac{\mathrm{d}\tau}{\sqrt{(\tau - c_r)(1 - \tau)}(\tau - \varsigma)}.$$

The last integral is evaluated as:

$$\frac{1}{\pi i} \int_{c_r}^{1} \frac{\mathrm{d}\tau}{\sqrt{(\tau - c_r)(1 - \tau)}(\tau - \varsigma)} = \frac{1}{\sqrt{(\varsigma - c_r)(1 - \varsigma)}}.$$

Finally, we get

$$w(\varsigma) = (q - k_2 b \sin \pi\alpha) \frac{\sqrt{(\varsigma - c_r)(1 - \varsigma)}}{\pi^2 i} \int_{c_r}^{1} \frac{(\log \tau - \log \varsigma)\, \mathrm{d}\tau}{\sqrt{(\tau - c_r)(1 - \tau)}(\tau - \varsigma)}$$
$$- \frac{k_2 b \sin \pi\alpha}{\pi} \log \varsigma + \frac{Q - q}{\pi} \log\left(m(\varsigma) + \sqrt{m(\varsigma)^2 - 1}\right) + iq. \tag{7}$$

Note, that the integral term in Eq. (7) exists as a usual improper integral.

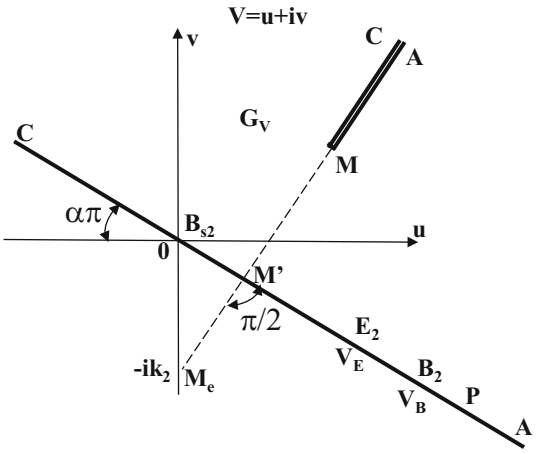


**Fig. 3** Hodograph domain for flow in Fig. 2a

Now we invert Eq. (1) as

$$\varsigma = \exp\left(-\pi z e^{i\pi\alpha}/b\right), \tag{8}$$

and put expression (8) into Eq. (7). This gives the expression $w(z)$.

An alternative hodograph method is used below as well; namely, the hodograph domain $G_V$ is shown in Fig. 3. $G_V$ has a cut CMA where $M$ is the point at which the velocity magnitude attains a minimum. The cut is perpendicular to the line $AB_2E_2B_{s2}C$ and its extension, the line $MM_1M_e$ passes through the point $M_e$ where $V = -ik_2$ and $M_1$ is the intersection of $MM_e$ with the straight line $AC$. The distance between points $M$ and $M_1$ is $d$. Obviously, $V = 0$ at the stagnation point $B_{s2}$.

We get a mirror image $G_\omega$ of $G_V$ with respect to the abscissa axis in Fig. 3. Obviously, $\omega(z) = \mathrm{d}w/\mathrm{d}z$ is a holomorphic function, $G_\omega$ and $G_w$ are triangles. First, we use the Schwarz–Chritoffel formula and map conformally $G_\omega$ onto the upper half of $\varsigma_1$-plane(Fig. 2d) by the function

$$\omega^*(\varsigma_1) = e^{i\pi\alpha}\left(k_2 \sin\pi\alpha + d\Big/\sqrt{\varsigma_1^2 - 1}\right), \tag{9}$$

where the radical's branch is fixed in the upper half plane being negative at $\varsigma_1 = \xi_1 < -1$. This function gives the following correspondence of boundary points: $(-\infty, \beta_s, -1, 0, 1, \sigma_1, \beta(d), \varepsilon(d, q)) \to (M', B_s, C, M, A, P, B, E)$. Obviously, from Eq. (9) applied at point $B_s$ we have $\beta_s(d) = -\sqrt{1 + d^2/(k_2 \sin\pi\alpha)^2}$.

Here, we save the same designations for the symmetric boundary points of the domains $G_\varpi$ and $G_V$,

$$\begin{aligned}
&\omega^*(\beta(d)) = e^{i\pi\alpha}Q/b, \quad \omega^*(\varepsilon(d,q)) = e^{i\pi\alpha}q/b, \text{ i.e.}\\
&\beta = \beta(d) = \frac{\sqrt{(Q - k_2 b\sin\pi\alpha)^2 + b^2d^2}}{Q - k_2 b\sin\pi\alpha} > 1,\\
&\varepsilon = \varepsilon(d,q) = \frac{\sqrt{(q - k_2 b\sin\pi\alpha)^2 + b^2d^2}}{q - k_2 b\sin\pi\alpha} > \beta.
\end{aligned} \tag{10}$$

Next, we use the Mőbius transformation to map the half plane in Fig. 1d onto one in Fig. 1c:

$$\varsigma_1(\varsigma) = \frac{(\varepsilon-1)\beta\varsigma - (\beta-1)\varepsilon}{(\varepsilon-1)\varsigma + 1 - \beta}, \quad \varsigma(\varsigma_1) = \frac{(\beta-1)(\varsigma_1-\varepsilon)}{(\varepsilon-1)(\varsigma_1-\beta)}. \tag{11}$$

Thus,

$$\frac{\mathrm{d}w}{\mathrm{d}z}(\varsigma) = \omega(\varsigma) = \omega^*(\varsigma_1(\varsigma)). \tag{12}$$

Note that the preimages of the points $C = \infty$ and $M = e^{i\pi\alpha}\,(k_2 \sin\pi\alpha - id)$ in the $\varsigma$-plane are

$$c_r = [(1+\varepsilon)(\beta-1)]/[(1+\beta)(\varepsilon-1)] \quad \text{and} \quad m_r = \varepsilon(\beta-1)/[\beta(\varepsilon-1)], \tag{13}$$

correspondingly.

In order to find $q$ we use the physical conditions at point P: $w_P = iQ - k_2 r_P \sin\alpha\pi$ and at point C: $w_C = iq + r\sin\alpha\pi$. The former follows from the piezometer readings and the latter—from the third condition (2) and Fig. 2a, b where C is the rim point of the seepage face.

We integrate Eq. (12) as:

$$w = iQ + \int_A^z \frac{\mathrm{d}w}{\mathrm{d}z}\mathrm{d}z = iQ + \int_1^\varsigma \frac{\mathrm{d}w}{\mathrm{d}z}(\varsigma)\frac{\mathrm{d}z}{\mathrm{d}\varsigma}\mathrm{d}\varsigma = iQ - \frac{be^{-i\pi\alpha}}{\pi}\int_1^\varsigma \omega(\varsigma)\frac{\mathrm{d}\varsigma}{\varsigma}. \tag{14}$$

In Eq. (14) we have expressed $\mathrm{d}z/\mathrm{d}\varsigma$ from Eq. (1) and $\mathrm{d}w/\mathrm{d}z$ from Eq. (9) through Eq. (12). At point C from Eq. (14) we get two relations:

$$q = Q - \mathrm{Im}\left[\frac{be^{-i\pi\alpha}}{\pi}\int_1^{c_r}\omega(\varsigma)\frac{\mathrm{d}\varsigma}{\varsigma}\right] = Q - \frac{b}{\pi}\int_1^{c_r}\mathrm{Im}\left[e^{-i\pi\alpha}\omega(\varsigma)\right]\frac{\mathrm{d}\varsigma}{\varsigma},$$

$$r\sin\pi\alpha = -\mathrm{Re}\left[\frac{be^{-i\pi\alpha}}{\pi}\int_1^{c_r}\omega(\varsigma)\frac{\mathrm{d}\varsigma}{\varsigma}\right] = -\frac{b}{\pi}k_2\sin\pi\alpha\ \mathrm{Log}\,c_r, \tag{15}$$

where Re and Im are the real and imaginary parts. To derive the latter relation (15) we have taken into account that $\omega(\varsigma)$ maps the interval $(c_r, 1)$ onto a cut along the ray (CMA) (see Fig. 3), i.e., $\mathrm{Re}\left[e^{-i\pi\alpha}\omega(\varsigma)\right] \equiv k_2\sin\pi\alpha$ for $\varsigma \in (c_r, 1)$.

We evaluate the integral in the first Eq. (15) as:

$$\int_1^{c_r}\mathrm{Im}\left[e^{-i\pi\alpha}\omega(\varsigma)\right]\frac{\mathrm{d}\varsigma}{\varsigma} = -d\int_1^{c_r}\frac{\mathrm{d}\varsigma}{\sqrt{1-\varsigma_1(\varsigma)^2}\,\varsigma} = d(\varepsilon-\beta)\int_{-1}^{1}\frac{\mathrm{d}\varsigma_1}{\sqrt{1-\varsigma_1^2}(\beta-\varsigma_1)(\varepsilon-\varsigma_1)}$$

$$= d\int_{-\pi/2}^{\pi/2}\left(\frac{1}{\beta-\sin\phi} - \frac{1}{\varepsilon-\sin\phi}\right)\mathrm{d}\phi = \pi d\left((\beta^2-1)^{-1/2} - (\varepsilon^2-1)^{-1/2}\right).$$

The last integral above was evaluated by formula (2.452, 10) from Gradshteyn and Ryzik (1980).

Thus, the first Eq. (15) is reduced to the following one $q = Q - bd((\beta^2-1)^{-1/2} - (\varepsilon^2-1)^{-1/2})$, which, in accordance with (10), is just the identity. The second relation (15), due to (10), (13), gives the equation

$$[(1+\varepsilon)(\beta-1)]/[(1+\beta)(\varepsilon-1)] = \exp\left(-\pi r/(K_2 b)\right), \quad \text{or}$$

$$\frac{q-k_2 b\sin\pi\alpha+\sqrt{(q-k_2 b\sin\pi\alpha)^2+b^2d^2}}{Q-k_2 b\sin\pi\alpha+\sqrt{(Q-k_2 b\sin\pi\alpha)^2+b^2d^2}}=\exp\left(-\frac{\pi r}{2k_2 b}\right). \tag{16}$$

At the point P from Eq. (14) we get:

$$k_2 h_P=\frac{be^{-i\pi\alpha}}{\pi}\int\limits_1^{\sigma}\omega(\varsigma)\frac{\mathrm{d}\varsigma}{\varsigma}. \tag{17}$$

because $w_p=\phi_P+iQ=-k_2h_P+iQ$. Due to (9), (12) the last integral is evaluated as follows

$$\frac{b}{\pi}\int\limits_1^{\sigma}\left(k_2\sin\pi\alpha+\frac{d}{\sqrt{\varsigma_1(\varsigma)^2-1}}\right)\frac{\mathrm{d}\varsigma}{\varsigma}$$
$$=\frac{b}{\pi}\left(k_2\sin\pi\alpha\ \mathrm{Log}\,\sigma+d\int\limits_1^{\sigma_1}\left(\frac{1}{\varsigma_1-\varepsilon}-\frac{1}{\varsigma_1-\beta}\right)\frac{\mathrm{d}\varsigma_1}{\sqrt{\varsigma_1^2-1}}\right).$$

After some algebra we get

$$\int\limits_1^{\sigma_1}\left(\frac{1}{\varsigma_1-\varepsilon}-\frac{1}{\varsigma_1-\beta}\right)\frac{\mathrm{d}\varsigma_1}{\sqrt{\varsigma_1^2-1}}=\int\limits_0^{\mathrm{Arccosh}\,\sigma_1}\left(\frac{1}{\cosh\phi-\varepsilon}-\frac{1}{\cosh\phi-\beta}\right)\mathrm{d}\phi$$
$$=\frac{2}{\sqrt{\beta^2-1}}\mathrm{ArcTanh}\left(\sqrt{\frac{\beta+1}{\beta-1}}\sqrt{\frac{\sigma_1-1}{\sigma_1+1}}\right)-\frac{2}{\sqrt{\varepsilon^2-1}}\mathrm{ArcTanh}\left(\sqrt{\frac{\varepsilon+1}{\varepsilon-1}}\sqrt{\frac{\sigma_1-1}{\sigma_1+1}}\right).$$

Here, $\sigma_1=\varsigma(\sigma)$ and in accordance with (11)

$$\frac{\sigma_1-1}{\sigma_1+1}=\frac{\beta-1}{\beta+1}\frac{\sigma-1}{\sigma-c_r},\quad \sigma=\exp(\pi r_p/b),\quad c_r=\frac{(\varepsilon+1)(\beta-1)}{(\varepsilon-1)(\beta+1)}.$$

Thus, Eq. (17) becomes

$$\frac{k_2\pi}{b}(h_P-r_P\sin\pi\alpha)=\frac{2(Q-k_2 b\sin\pi\alpha)}{b}\mathrm{ArcTanh}\left(\sqrt{\frac{\exp(\pi r_p/b)-1}{\exp(\pi r_p/b)-\exp(-\pi r/b)}}\right)$$
$$-\frac{2(q-k_2 b\sin\pi\alpha)}{b}\mathrm{ArcTanh}$$
$$\times\left(\sqrt{\exp(-\pi r/b)\frac{\exp(\pi r_p/b)-1}{\exp(\pi r_p/b)-\exp(-\pi r/b)}}\right). \tag{18}$$

From (18) we express $q$ through the physical and geometrical parameters.

We introduce dimensionless variables as $(z^*, r^*, r_P^*, h_P^*=z/b, r/b, r_P/b, h_P/b)$, $(w^*, q^*, Q^*)=(w/(k_2b), q/(k_2b), Q/(k_2b))$, $(d^*, V^*)=(d/k_2,\ V/k_2)$ and drop the subscript * for the sake of brevity.

Figure 4 shows the graphs $q(r)$ at $Q=0.2$, $r_P=1.0$, $h_P=1.0$ and $\alpha=0.08$, 0.1 and 0.12 (curves 1–3). As we can see from these curves, the increase in the size of the window significantly reduces the value of $q$. At $r=0.52$, 0.19 and 0.08, calculated by the **FindRoot** routine of *Mathematica* (Wolfram 1991), $q$ vanishes, i.e., the flow regime in Fig. 2a is not valid anymore at higher values of $r$, when a part of the "window" near point C becomes a

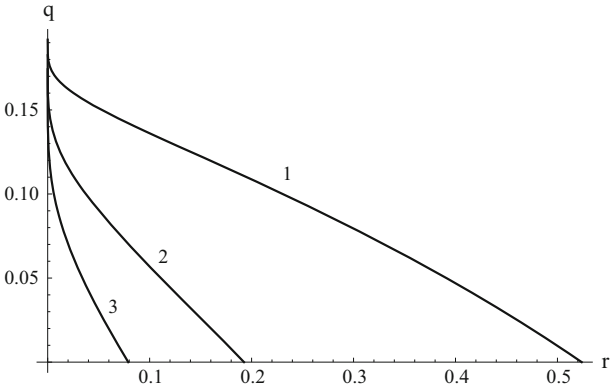


**Fig. 4** Flow rate through a bedrock window for $Q = 0.2$, $r_P = 1.0$, $h_P = 1.0$ and $\alpha = 0.08$, 0.1 and 0.12 (curves *1–3*)

losing rather than gaining isobar as in Toth (2009). Therefore, the flow topology, hodograph and complex potential domains shown in Figs. 2, 3 have to be changed.

## 3 Unconfined Flow with Losses to a Seepage Face in Bedrock

In this section we analyze a phreatic surface flow in the upper aquifer (Fig. 1), close to the "window" GF through which groundwater is completely drained to aquifer 2 (Bush's submergence, see the epigraph). The corresponding analytic element is zoomed in Fig. 5a.

We introduce Cartesian coordinates $xGy$. Because $k_2 \gg k_1$ all water is freely drained into the substratum and the breach GN is a seepage face for flow in aquifer 1. The locus of point N is a part of solution as well as the shape of the free surface. The main question is: at which magnitude of the incident velocity $V_I$ the inequality holds: $R_N < R_F$?

The flow domain $G_z$ is bounded by an impermeable ray $I_1G$, free surface $I_2N$ and isobar GN. The magnitude of the Darcian velocity far upstream of the window is $|V_I| = k_1 \sin^2 \alpha$ and the flow rate $Q_I = BV_I = k_1 B \sin \alpha$ where $B$ is the normal depth of the incident flow upstream of GN (see Kacimov et al. 2015 for definition of normal flow conditions). If $Q_I$ is small enough or the width of the window is large enough, then the whole incident flow is intercepted by the seepage face. Otherwise, we will have both drainage through the whole segment GF and a "thinner" flow downstream of F, with a separatrix similar to one in the previous section. We will not analyze the latter regime.

The hodograph domain $G_V$ is depicted in Fig. 5b. It represents a circular triangle whose side, the ray NG is perpendicular to the side $I_1G$, which is also a ray. Obviously, NG passes also through the point $(0, -ik_1)$ of the hodograph plane. The side $I_2N$ of $G_V$ is an arc of a circle centered at the point $(0, -ik_1/2)$ and of diameter $k_1$. Clearly, in $G_V$ the points $I_2$ and $I_1$ merge into one point. At point $G$ velocity is infinite as at points $A$ and $C$ in Figs. 2a and 3.

The complex potential domain $G_w$ is shown in Fig. 5c. $G_w$ is a half strip of width $Q$ with a curved side $GN$.

The BVP is:

$$I_1G_1 : \psi = 0, \qquad y = -x \tan \pi\alpha,$$
$$I_2N : \varphi + k_1 y(\xi) = 0, \quad \psi = Q_I,$$

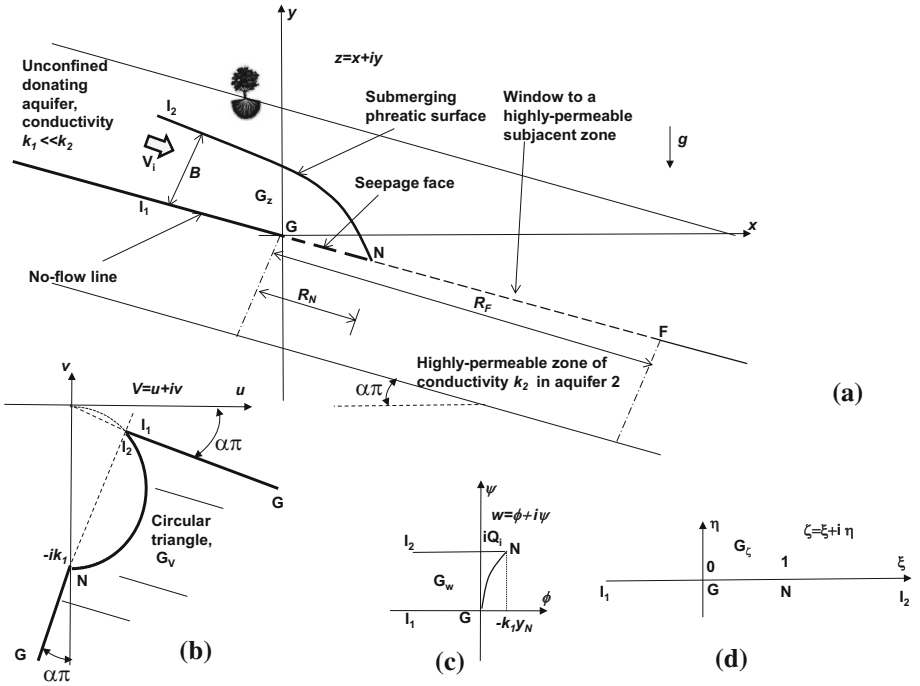


**Fig. 5** Unconfined aquifer discharging through a bedrock window: physical flow domain (**a**), hodograph domain (**b**), complex potential domain (**c**), auxiliary plane (**d**)

$$\mathrm{GN}: \ \varphi + k_1 y(\xi) = 0, \quad y = -x \tan \pi\alpha. \tag{19}$$

In terms of functions $F(\varsigma) = \mathrm{d}w/\mathrm{d}\varsigma$ and $Z(\varsigma) = \mathrm{d}z/\mathrm{d}\varsigma$ the boundary conditions (19) applied in the upper half plane of an auxiliary $\varsigma$-plane (Fig. 4d) are expressed as:

$$\begin{aligned}
&\mathrm{Im}\ F(\xi) = 0, \quad \mathrm{Im}\left[e^{i\pi\alpha} Z(\xi)\right] = 0, \quad -\infty < \xi < 0;\\
&\mathrm{Im}\left[i F(\xi) + k_1 Z(\xi)\right] = 0, \quad \mathrm{Im}\left[e^{i\pi\alpha} Z(\xi)\right] = 0, \quad 0 < \xi < 1;\\
&\mathrm{Im}\left[i F(\xi) + k_1 Z(\xi)\right] = 0, \quad \mathrm{Im}\ F(\xi) = 0, \quad 1 < \xi < \infty.
\end{aligned} \tag{20}$$

Thus, for a vector function $\mathbf{X}(\varsigma) = (F(\varsigma), Z(\varsigma))$ we have a matrix Riemann boundary value problem: $\mathrm{Im}\left\lfloor \mathbf{X}(\xi) M_j \right\rfloor = 0, \quad \xi \in l_j, j = 1, 2, 3$. Here, $l_1 = (-\infty, 0)$, $l_2 = (0, 1)$, $l_3 = (1, \infty)$, and matrices are:

$$M_1 = \begin{Vmatrix} 1 & 0 \\ 0 & e^{i\pi\alpha} \end{Vmatrix}, \quad M_2 = \begin{Vmatrix} i & 0 \\ k_1 & e^{i\pi\alpha} \end{Vmatrix}, \quad M_3 = \begin{Vmatrix} i & 1 \\ k_1 & 0 \end{Vmatrix}.$$

Now we introduce new unknown vector functions

$$\mathbf{X}_1(\varsigma) = \mathbf{X}(\varsigma) M_1, \quad \mathbf{X}_2(\varsigma) = \left\{ \mathbf{X}_1(\varsigma), \mathrm{Im}\ \varsigma > 0; \ \overline{\mathbf{X}_1(\bar{\varsigma})}, \mathrm{Im}\ \varsigma < 0 \right\} \tag{21}$$

and jump from the BVP (10) to the Hilbert BVP:

$$\mathbf{X}_2^+(\xi) = \mathbf{X}_2^-(\xi) L_j, \quad \xi \in l_j, \quad j = 1, 2, 3, \tag{22}$$

where matrices $L_j = \overline{M_1^{-1}}\overline{M_j}M_j^{-1}M_1$ are

$$L_1 = \begin{Vmatrix} 1 & 0 \\ 0 & 1 \end{Vmatrix}, \quad L_2 = \begin{Vmatrix} -1 & 0 \\ 2k\sin\pi\alpha & 1 \end{Vmatrix}, \quad L_3 = \begin{Vmatrix} 1 & -2ie^{i\pi\alpha}/k_1 \\ 0 & e^{i2\pi\alpha} \end{Vmatrix}.$$

We use the matrix

$$S = \begin{Vmatrix} -k_1\sin\pi\alpha & 0 \\ k_1\sin\pi\alpha & 1 \end{Vmatrix} \tag{23}$$

and the substitution $\mathbf{X}_2(\xi) = \mathbf{X}_3(\xi)S$. We get the following Hilbert BVP for the vector function $\mathbf{X}_3 = (X_{31}, X_{32})$: $\mathbf{X}_3^+(\xi) = \mathbf{X}_3^-(\xi)$, $-\infty < \xi < 0$;

$$\begin{cases} X_{31}^+(\xi) = -X_{31}^+(\xi) \\ X_{32}^+(\xi) = X_{32}^-(\xi) \end{cases}, \ 0 < \xi < 1; \quad \begin{cases} X_{31}^+(\xi) = e^{i2\pi\alpha}X_{31}^-(\xi) \\ X_{32}^+(\xi) = \left(e^{i2\pi\alpha} - 1\right)X_{31}^-(\xi) + X_{32}^-(\xi) \end{cases}, \ 1 < \xi < \infty. \tag{24}$$

This problem has to be solved in the class of holomorphic functions with integrable singularities at the points $\varsigma = 0$, $\varsigma = 1$, vanishing at infinity and satisfying the symmetry condition:

$\overline{\mathbf{X}_3(\bar{\varsigma})} \equiv \mathbf{X}_3(\xi)$. The last relation follows from the definition (21) and reality of the matrix (23).

Note that if solution to the problem (24) is found, then a solution of the initial problem (20) will follow from the relation $\mathbf{X}(\varsigma) = \mathbf{X}_3(\varsigma)\mathrm{S}\mathrm{M}_1^{-1}$ (see Eqs. (20), (22, (23)). Thus,

$$F(\varsigma) = k_1\sin\pi\alpha\,(X_{32}(\varsigma) - X_{31}(\varsigma)), \quad Z(\varsigma) = e^{-i\pi\alpha}X_{32}(\varsigma). \tag{25}$$

Let us consider the function

$$X_{31}(\varsigma) = c(-\varsigma)^{-1/2}(1-\varsigma)^{-1/2-\alpha}, \tag{26}$$

a single-valued branch of which is fixed in the $\varsigma-$plane with the cut along the positive part of the real axis by the conditions $-\pi < \arg(-\varsigma) < \pi$, $-\pi < \arg(1-\varsigma) < \pi$. It is clear that $X_{31}(\varsigma)$ meets all above required conditions if $c$ is an arbitrary real constant. Due to Eqs. (24), (26) the second component $X_{32}(\varsigma)$, as a solution of the jump problem

$$X_{32}^+(\xi) - X_{32}^-(\xi) = (e^{i2\pi\alpha} - 1)X_{31}^-(\xi), \quad 1 < \xi < \infty,$$

is given now by the Cauchy-type integral

$$\begin{aligned} X_{32}(\varsigma) &= -\frac{c\,\sin\pi\alpha}{\pi}\int_1^\infty \tau^{-1/2}(\tau-1)^{-1/2-\alpha}\frac{\mathrm{d}\tau}{\tau-\varsigma} \\ &= -\frac{c\,\sin\,\pi\alpha}{\pi}\int_0^1 \tau^{\alpha}(1-\tau)^{-1/2-\alpha}\frac{\mathrm{d}\tau}{1-\tau\varsigma}. \end{aligned} \tag{27}$$

In order to derive the last integral representation, we took into account that $X_{31}^-(\tau) = -ce^{-i\pi\alpha}\tau^{-1/2}(\tau-1)^{-1/2-\alpha}$ for $\varsigma = \tau > 1$, and used the substitution $\tau \to 1/\tau$. The integral in Eq. (27) can be expressed in terms of a hypergeometric function:

$$\begin{aligned} X_{32}(\varsigma) &= \frac{2c\Gamma(0.5-\alpha)}{\sqrt{\pi}\Gamma(-\alpha)}F(1, 1+\alpha; 1.5; \varsigma) \\ &= \frac{2c\Gamma(0.5-\alpha)}{\sqrt{\pi}\Gamma(-\alpha)}(1-\varsigma)^{-1/2-\alpha}F(0.5, 0.5-\alpha; 1.5; \varsigma), \quad |\varsigma| < 1. \end{aligned} \tag{28}$$

Using analytical continuations of the hypergeometric function into vicinities of points $\varsigma = 1$ and $\varsigma = \infty$ we get

$$X_{32}(\varsigma) = c\frac{\Gamma(-0.5-\alpha)}{\sqrt{\pi}\Gamma(-\alpha)}F(1, 1+\alpha; 1.5+\alpha; 1-\varsigma) - c\tan\pi\alpha\,\varsigma^{-1/2}(1-\varsigma)^{-1/2-\alpha}, \quad |\varsigma - 1| < 1, \tag{29}$$

$$X_{32}(\varsigma) = c\frac{\Gamma(0.5-\alpha)}{\sqrt{\pi}\Gamma(1-\alpha)\varsigma}F(1, 0.5; 1-\alpha; 1/\varsigma) + c(-\varsigma)^{-1/2}(1-\varsigma)^{-1/2-\alpha}, \quad |\varsigma| > 1, \tag{30}$$

correspondingly. In Eqs. (28)–(30) $F$ is a hypergeometric function ${}_1F_2$, and $\Gamma$ is the Gamma function.

The required solution of problem (19) is defined now via Eqs. (25)–(30). The real parameter $c$ is evaluated from the relation $\mathrm{Im}\int\limits_0^1 F(\xi)\mathrm{d}\xi = Q_1$.

In accordance with Eqs. (16), (17), (19) we have

$$\mathrm{Im}\ F(\xi) = -ck_1\sin\ \pi\alpha\,\xi^{-1/2}(1-\xi)^{-1/2-\alpha}, \quad 0 < \xi < 1.$$

Due to formula (8.380, 1) from Gradshteyn and Ryzik (1980), we get

$$\mathrm{Im}\int\limits_0^1 F(\xi)\,\mathrm{d}\xi = \int\limits_0^1 \mathrm{Im}\ F(\xi)\,\mathrm{d}\xi = -c\sqrt{\pi}k_1\sin\ \pi\alpha\ \ \Gamma(0.5-\alpha)/\,\Gamma(1-\alpha);$$

then,

$$c = c(\alpha) = -Q_I\Gamma(1-\alpha)/[k_1\sqrt{\pi}\,\sin\pi\alpha\Gamma(0.5-\alpha)]. \tag{31}$$

We introduce dimensionless variables as $z^* = zk_1/Q_I$ and drop the subscript * for the sake of brevity. Then, using Eqs.(18), (19) and (21), the parametric equations of the segment $GN$ become:

$$z(\varsigma) = -\frac{\Gamma(1-\alpha)e^{-i\pi\alpha}}{\sqrt{\pi}\,\sin\pi\alpha\Gamma(0.5-\alpha)}\int\limits_0^{\zeta} X_{32}(\varsigma)\mathrm{d}\varsigma, \quad 0 < \varsigma < 1. \tag{32}$$

In particular, from Eq. (32) at $\varsigma = 1$ we get $z_N$. Then, $R_N = \mathrm{Im}[z_N/\cos\pi\alpha]$. We use Wolfram's *Mathematica* routines **Hypergeometric2F1**, **Gamma**, **NIntegrate** and **ParametricPlot**. Figure 6 shows the graph $R_N(\alpha)$. Consequently, if $R_F$ in Fig. 5a is less than what is presented in Fig. 6 there will be a "phreatic tail" downstream of GN.

Obviously, at $\alpha \to 0$ we get the Pavlovsky limit $R_N = 0.5$. In this case of a horizontal bedrock, there is no "normal" undisturbed flow parallel to the bedrock, i.e., groundwater at infinity is quiescent. The Pavlovsky's phreatic surface is a parabola. At another limit of $\alpha = 1/2$, flow in Fig. 5a degenerates into a 1D vertical jet, within which pressure is everywhere atmospheric and velocity is constant. Therefore, in this limit $I_1GN$ in Fig. 5a is both a streamline and isobar, i.e., another phreatic surface. Hence, $\lim\limits_{\alpha\to 1/2} R_N \to \infty$, as is evident from Fig. 6.

Next, for $NI_2$ from Eq. (28)–(32) we get

$$z(\varsigma) = z_N - \frac{\Gamma(1-\alpha)e^{-i\pi\alpha}}{\sqrt{\pi}\,\sin\pi\alpha\Gamma(0.5-\alpha)}\int\limits_1^{\zeta} X_{32}(\varsigma)\mathrm{d}\varsigma, \quad \zeta > 1. \tag{33}$$

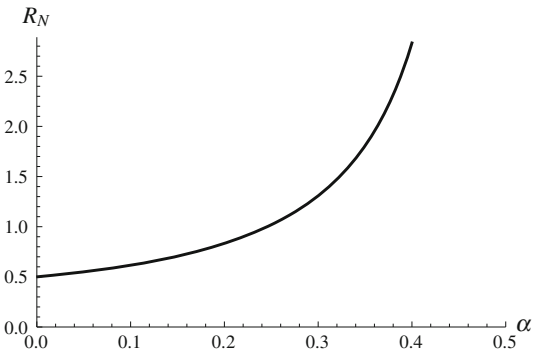


**Fig. 6** The size $R_N$ of GN in Fig. 4a as a function of angle $\alpha$ of sloping aquifer

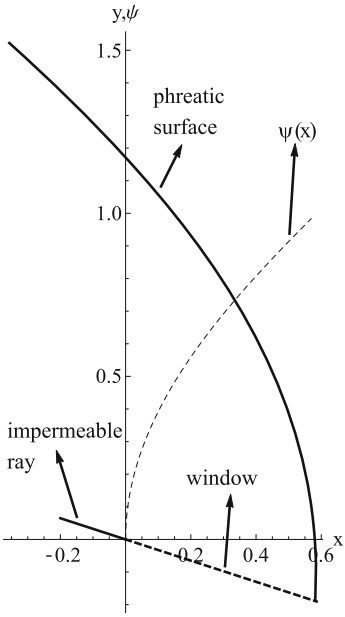


**Fig. 7** Phreatic surface and distribution of the stream function with $x$ for $\alpha = 0.1$

We used the *Mathematica* routines **Re** and **Im** and **ParametricPlot** to plot the phreatic surface $NI_2$ for $\alpha = 0.1$ (Fig. 7) where the thick dashed line represents the isobaric window $GN$. The thin dashed line in Fig. 7 shows the stream function $\psi(x)$ which was evaluated by integration of the first equation in Eq. (25).

## 4 Hydraulic Approximation for Flow in Two Commingled Aquifers

PK-62, 77 categorized models of phreatic flows as "hydrodynamic" and "hydraulic." The previous section dealt with the former and in this section we will produce a hydraulic, 1D solutions for the phreatic surface flow in the upper aquifer (Fig. 1), close to the drainage window GF through which groundwater is completely drained to aquifer 2. This is a stringent test case for 1D solutions, given the strongly curved free surface in Fig. 7 during the drainage to aquifer 2. We produce the second-order hydraulic theory following Picard's iteration,

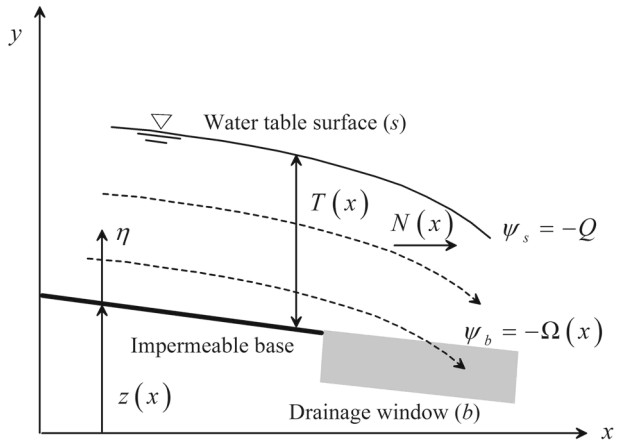


**Fig. 8** Notation for 1D flow solutions relevant to Fig. 4a

as used by Castro-Orgaz et al. (2012), Castro-Orgaz and Hager (2014) and Kacimov et al. (2015).

We recall that the Cartesian velocity components $u(x,\ y)$ and $v(x,\ y)$ of the potential flow (see Sects. 2, 3) obey the Cauchy–Riemann conditions (Bear 1972)

$$u = -\frac{\partial \phi}{\partial x} = -\frac{\partial \psi}{\partial y}, \quad v = -\frac{\partial \phi}{\partial y} = +\frac{\partial \psi}{\partial x}, \tag{34}$$

where the potential and stream functions are $\phi$ and $\psi$, respectively. The flow problem is sketched in Fig. 8, where an upstream curved seepage of constant discharge $Q$ is drained progressively across a permeable window (shaded area). The saturated thickness is $T(x)$ and the local seepage flow rate $N(x)$. The physical mechanism of such leakage can be different from what we studied in Sect. 3, i.e., instead of a highly permeable substratum the window can be made of a material less permeable than the main aquifer but more permeable than the aquifuge (bedrock) upstream of point $G$ (Fig. 4a).

Integration of the first of Eq. (34) in the vertical direction with $x$ as constant and the variable $\eta(x,\ y) = y - z(x)$ as the vertical distance above the bottom yields

$$\psi = -\int u \mathrm{d}\eta + g\,(x) = -U\eta - \Omega\,(x)\,, \tag{35}$$

where the bed condition for the stream function $\psi_b = -\Omega\ (x)$ was used to find the integration function $g(x)$. The depth-averaged velocity $U = N/T$ is selected as a starting function in Eq. (35). Using Eq. (35) $v$ is

$$v = \psi_x = -U_x\eta - U\eta_x - \Omega_x. \tag{36}$$

From Eq. (36) with $f$ as arbitrary function of $x$ we get

$$-\phi = \int v \mathrm{d}\eta + f\,(x) = -U_x\frac{\eta^2}{2} - U\eta\eta_x - \eta\Omega_x + f\,(x)\,. \tag{37}$$

Now,

$$u = -\phi_x = -U_{xx}\frac{\eta^2}{2} - (2U_x\eta_x + U\eta_{xx})\,\eta - U\eta_x^2 + f_x - \Omega_{xx}\eta - \Omega_x\eta_x, \tag{38}$$

where $f_x$ remains unknown. Integration of Eq. (38) yields

$$\psi = -\int u\mathrm{d}\eta + \beta(x) = U_{xx}\frac{\eta^3}{6} + (2U_x\eta_x + U\eta_{xx})\frac{\eta^2}{2} + U\eta_x^2\eta - f_x\eta + \Omega_{xx}\frac{\eta^2}{2} + \Omega_x\eta_x\eta + \beta(x), \tag{39}$$

where $\beta(x)$ is an arbitrary function. Equation (39) is used to obtain $f_x$ subject to the boundary condition of the stream function at the free surface and bed surfaces, that is,

$$\begin{aligned} \psi_s[\eta = T(x)] &= -Q, \\ \psi_b[\eta = 0] &= -\Omega(x). \end{aligned} \tag{40}$$

Inserting Eq. (40) into Eq. (39) gives

$$f_x = U + U_{xx}\frac{T^2}{6} + (2U_x\eta_x + U\eta_{xx})\frac{T}{2} + U\eta_x^2 + \Omega_{xx}\frac{T}{2} + \Omega_x\eta_x. \tag{41}$$

Using (41) into Eq. (38) produces the velocity profile

$$u = U + (2U_x\eta_x + U\eta_{xx} + \Omega_{xx})\left(\frac{T}{2} - \eta\right) + U_{xx}\left(\frac{T^2}{6} - \frac{\eta^2}{2}\right). \tag{42}$$

The velocity vector in seepage flow is assumed to follow Darcy's law in isotropic and homogeneous porous media. Based on the definition of the hydraulic head $h$ Eq. (37) is rewritten as

$$-Kh = -U_x\frac{\eta^2}{2} - U\eta\eta_x - \Omega_x\eta + f(x). \tag{43}$$

At the water table surface the pressure is atmospheric, so that (43) gives

$$-K(T+z) = -U_x\frac{T^2}{2} - UT\eta_x - \Omega_x T + f(x). \tag{44}$$

This is solved for $f$ and then back-substituted into (43) to provide

$$-Kh = \frac{U_x}{2}\left(T^2 - \eta^2\right) + (U\eta_x + \Omega_x)(T - \eta) - K(T + z). \tag{45}$$

Equation (45) is differentiated to obtain the horizontal velocity component $u$ as

$$u = -Kh_x = -K(T_x + z_x) + \frac{U_{xx}}{2}\left(T^2 - \eta^2\right) + (U\eta_{xx} + U_x\eta_x + \Omega_{xx})(T - \eta) + (T_x - \eta_x)(U\eta_x + \Omega_x) + U_x(TT_x - \eta\eta_x). \tag{46}$$

Equation (42) at the water table yields

$$u_s = U - (2U_x\eta_x + U\eta_{xx} + \Omega_{xx})\frac{T}{2} - U_{xx}\frac{T^2}{3}, \tag{47}$$

whereas from Eq. (46)

$$u_s = -K(T_x + z_x) + (T_x - \eta_x)(U\eta_x + \Omega_x) + U_xT(T_x - \eta_x). \tag{48}$$

Equaling (47) and (48) provides the ODE describing the water table to second-order accuracy as

$$U-\left[\left(UT_x\eta_x-U\eta_x^2+\frac{U\eta_{xx}T}{2}\right)+\left(U_xT_xT+U_{xx}\frac{T^2}{3}\right)\right.$$
$$\left.+\left((T_x-\eta_x)\,\Omega_x+\frac{\Omega_{xx}T}{2}\right)\right]+K\,(T_x+z_x)=0. \tag{49}$$

Expressing $U$ and $\eta$ as a function of the variables $N$, $T$ and $z$ one finds

$$U_x=\frac{N_x}{T}-\frac{NT_x}{T^2},\quad U_{xx}=\frac{N_{xx}}{T}-\frac{NT_{xx}}{T^2}+2\frac{NT_x^2}{T^3}-2\frac{N_xT_x}{T^2},$$
$$\eta_x=-z_x,\quad \eta_{xx}=-z_{xx}, \tag{50}$$

and inserting the result into Eq. (49) gives

$$\frac{N}{T}\left(1+T_xz_x+z_x^2+\frac{Tz_{xx}}{2}+\frac{TT_{xx}+T_x^2}{3}-\frac{N_xT_xT}{3N}\right.$$
$$\left.-\frac{N_{xx}T^2}{3N}-(T_x+z_x)\,\frac{\Omega_xT}{N}-\frac{\Omega_{xx}T^2}{2N}\right)+K\,(T_x+z_x)=0. \tag{51}$$

Equation (51) reduces to the Dupuit–Forchheimer theory if $T_xz_x$, $z_x^2$, $TT_{xx}$, $Tz_{xx}$, $T_x^2$, $N_xT_x$, $\Omega_xT_x$, $\Omega_{xx}T^2$ and $N_{xx}T^2$ are zero, leading to

$$\frac{N}{T}+K\,(T_x+z_x)=0, \tag{52}$$

which is presented in PK (Chapter X, Eq. 5.1). For constant discharge $q=Q$ (no leakage losses to aquifer 2) on a constant bed slope Eq. (51) reduces to

$$\frac{Q}{T}\left(1+T_xz_x+z_x^2+\frac{TT_{xx}+T_x^2}{3}\right)+K\,(T_x+z_x)=0, \tag{53}$$

which was solved by Kacimov et al. (2015). For the flow problem depicted in Fig. 8 conservation of mass gives

$$N\,(x)=-\,(\psi_s-\psi_b)=Q-\Omega\,(x)\,, \tag{54}$$

from which follows

$$N_x=-\Omega_x,\quad N_{xx}=-\Omega_{xx}. \tag{55}$$

Inserting (55) into Eq. (51) gives the ODE

$$\frac{N}{T}\left(1+T_xz_x+z_x^2+\frac{Tz_{xx}}{2}+\frac{TT_{xx}+T_x^2}{3}+\frac{N_{xx}T^2}{6N}+\left(\frac{2}{3}T_x+z_x\right)\frac{N_xT}{N}\right)$$
$$+K\,(T_x+z_x)=0, \tag{56}$$

which is a generalization of the development of Kacimov et al. (2015).

To test the validity of 1D solutions in this limiting test case Eq. (56) was integrated numerically using a fourth-order Runge–Kutta method (Press et al. 2007) for the same test case previously presented in Fig. 7 ($z_{xx}=0$). Equation (56) was transformed into a system of 2 ODEs for $T\,(x)$ and $T_x\,(x)$. The boundary section was taken at the first 2D point in Fig. 7, and the values of $T$ and $T_x$ deduced from the 2D results at that section were taken for the 1D solution. To give closure to Eq. (56) $\Omega\,(x)$ must be prescribed. Two-dimensional results for $\psi_b$ in Fig. 7 are almost perfectly matched by a function proportional to $x^{1/2}$. However, gradients of $N_x$ and $N_{xx}$ would then tend to infinity at $x=0$, breaking down 1D computations. Thus, the simplest approach for 1D modeling was used assuming a linear distribution of $\psi_b$ along the drainage window. It automatically gives $N_{xx}=0$ and a constant intensity $N_x$.

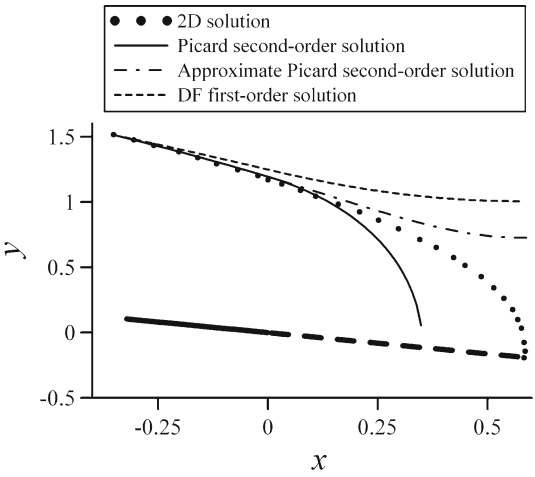


**Fig. 9** Comparison of 1D and 2D solutions

The results of the computation are presented in Fig. 9. It can be observed that in the constant discharge domain ($x < 0$) the solution of Eq. (56) is in good agreement with 2D data. Once the flow enters into the drainage window area the 1D simulations agrees with 2D data up to $x = 0.2$, roughly. After that point the interaction of $N_x$ and $(2/3T_x)$ in Eq. (56) provokes an excessive slope of the phreatic surface, that ultimately becomes vertical at point N (see the hodograph in Fig. 4b) that violates the very premise of the hydraulic theory (slope of the phreatic surface is "mild" in the sense of deviation from the bedrock slope, see PK). In other words, the approximation breaks at about $x = 0.35$. It means that higher-order expansions are needed in this flow zone of intense vertical motion. To elucidate the role of $N_x$ Eq. (56) was solved setting $N_x$ and $N_{xx}$ to zero. The equation was then solved with the same method and subjected to identical boundary conditions, and the results are plotted in Fig. 9 and labeled as "approximate Picard second-order solution." It can be observed that this computations is in agreement with the former Picard solution up to $x = 0.2$. In other words, the effect of $N_x$ is not significant upstream of that coordinate. In contrast, for $x > 0.2$ Fig. 9 suggest that $N_x$ controls the shape of the solution. None of the computations succeed in producing an accurate 1D flow profile, but this critical comparison suggests that a higher-order solution with a more accurate treatment of $N_x$ is needed. The standard DF theory given by Eq. (52) was also solved, and the results are presented in Fig. 9. As observed, this theory is not in agreement with 2D data in any part of the computational domain. Therefore, the second-order hydraulic theory is an improvement over DF theory, given that a good solution is found for $x < 0.2$. For $0.2 < x < 0.6$, 1D solutions were found to diverge from the 2D "exact" solution, and higher-order solutions are needed.

## 5 Conclusions

Groundwater flows in hillslope hydrology of commingled aquifers–aquitards are vitally important for water deficient countries such as Oman where mountains (Jabel Shams, Jabel Al-Akdar, Jabel Qara and others) serve as regional interceptors and condensers of rainfall which naturally replenishes strategic aquifers. We often encountered "strange" cases when a "normal"—in the sense of channel hydraulics (Chow 1959)—groundwater flow in a seemingly simple aquifer with a constant slope suddenly disappears. Similarly, groundwater re-emerges (sometimes as a spring, see, e.g., Al-Amri 2006) from below in a hydrostrati-

graphic unit (e.g., a relatively dry soil layer), which few hundred meters upstream is dry. This paper explains these anomalies by detouring a standard concept of layered aquifers–aquitards–aquifuges having flat interfaces between the layers and no variations of hydraulic properties along the layers.

In this paper, we extended the very concept of a hydrostratigraphic unit. In the past we studied nonstandard aquifers, i.e., ones with slope changes, anticlines, groundwater falls, imbedded lenses of contrasting permeability (Kacimov 2012; Kacimov and Obnosov 2000, 2008; Kacimov et al. 2015). Here, we assumed that the caprock or bedrock of a confined or unconfined aquifer is not an impervious surface but has a breach of a finite width. This tilted isobaric boundary serves as "window" through which groundwater either dives to a subjacent aquifer or vents to a superjacent one. Groundwater flows in sloping aquifers are commonly tackled by numerical codes (Broda et al. 2011; Dusek and Vogel 2014), with MODFLOW or HYDRUS3D involved. Analytical solutions are available for DF (Youngs and Rushton 2009; Rushton and Youngs 2010; Castro-Orgaz and Hager 2014) approximations (PK). In this paper we used and compared the results of a full potential 2D model based on solution of the Laplace equation and extended 1D model with extra terms added to the DF approximation, where the governing nonlinear ODE is solved. We engaged a full spectrum of analytical techniques: the hodograph method with conformal mappings, integral solutions to the Riemann–Hilbert BVP and Picard iterations.

We generalized the classical Pavlovsky problem of phreatic flow to a Zhukovskii toe drain placed on a horizontal bedrock, the problem of great importance in geotechnical engineering of earth-filled dams (PK); namely, we found how the Pavlovsky parabola metamorphizes into a bedrock-aligned curve when the bedrock is tilted at a constant angle. We also showed what happens with the PK and Numerov solutions to the problem of inflow, outflow or through flow from/to a constant head breach in a confined aquifer if the aquifer is inclined and the breach is a seepage face rather than a constant head segment.

**Acknowledgments** This work was funded by SQU, Grant SR/SCI/ETHS/11/01, Russian Foundation for Basic Research Grant No. 13-01-00322 and through a special program of the Russian Government supporting research at Kazan Federal University.

**Conflict of interest** The authors declare that they have no conflict of interest.

**Human and Animal Rights** There are no Human Participants and/or Animals and according to the institutional codes of the three universities, which the authors are affiliated with (Kazan Federal University—Russia, Sultan Qaboos University—Oman and University of Cordoba—Spain) this work does not require a special clearance of a Clinical Medicine and/or Animal Treatment committees.

## References

Al-Amri, M.: Hydrologic and hydrogeologic responses of springs to rainfall in Garsias and Arzat upper catchments. M.Sc. Thesis. Sultan Qaboos University, Muscat (2006)

Aravin, V.I., Numerov, S.N.: Theory of Fluid Flow in Undeformable Porous Media. Gostekhizdat, Moscow (1953). Translated Israel Program for Scientific Translation, Jerusalem (1965) (in Russian)

Bear, J.: The Dynamics of Fluids in Porous Media. Elsevier, New York (1972)

Bense, V.F., Gleeson, T., Loveless, S.E., Bour, O., Scibek, J.: Fault zone hydrogeology. Earth Sci. Rev. **127**, 171–192 (2013)

Broda, S., Paniconi, C., Larocque, M.: Numerical investigation of leakage in sloping aquifers. J. Hydrol. **409**, 49–61 (2011)

Castro-Orgaz, O., Giráldez, J.V., Robinson, N.: Second order two-dimensional solution for the drainage of recharge based on Picard's iteration technique: a generalized Dupuit–Forchheimer equation. Water Resour. Res. **48**, W06516 (2012). doi:10.1029/2011WR011751

Castro-Orgaz, O., Hager, W.H.: 1D modelling of curvilinear free surface flow: generalized Matthew theory. J. Hydraul. Res. **52**(1), 14–23 (2014)
Chow, V.T.: Open-Channel Hydraulics. McGraw-Hill, New York (1959)
Dusek, J., Vogel, T.: Modeling subsurface hillsloperunoffdominated by preferential flow: one-vs. two-dimensional approximation. Vadose Zone J. (2014). doi:10.2136/vzj2013.05.0082
Gabrielli, C.P., McDonnell, J.J., Jarvis, W.T.: The role of bedrock groundwater in rainfall-runoff response at hillslope and catchment scales. J. Hydrol. **450–451**, 117–133 (2012)
Gakhov, F.D.: Boundary Value Problems. Pergamon Press, Oxford (1966)
Gassiat, C., Gleeson, T., Lefebvre, R., McKenzie, J.: Hydraulic fracturing in faulted sedimentary basins: numerical simulation of potential contamination of shallow aquifers over long time scales. Water Resour. Res. **49**, 8310–8327 (2013). doi:10.1002/2013WR014287
George, R.J., Conacher, A.J.: Interactions between perched and saprolite aquifers on a small, salt-affected and deeply weathered hillslope. Earth Surf. Process. Landf. **18**, 91–108 (1993)
Gradshteyn, I.S., Ryzik, I.M.: Table of Integrals, Series and Products. Academic Press, New York (1980)
Hardie, M.A., Doyle, R.B., Cotching, W.E., Lisson, S.: Subsurface lateral flow in texture-contrast (duplex) soils and catchments with shallow bedrock. Appl. Environ. Soil Sci. **2012**, 10 (2012). doi:10.1155/2012/861358
Harte, P.T., Winter, T.C.: Simulations of flow in crystalline rock and recharge from overlying glacial deposits in a hypothetical New England setting. Groundwater **33**(6), 953–964 (1995)
Hemker, C.J.: Steady groundwater flow in leaky multiple aquifer systems. J. Hydrol. **72**, 355–374 (1984)
Iwagami, S., Tsujimura, M., Onda, Y., Shimada, J., Tanaka, T.: Role of bedrock groundwater in the rainfall-runoff process in a small headwater catchment underlain by volcanic rock. Hydrol. Process. **24**(19), 2771–2783 (2010). doi:10.1002/hyp.7690
Kacimov, A.R., Obnosov, Y.V.: Two-dimensional seepage in porous media with heterogeneities. J. Geochem. Explor. **69–70**, 251–255 (2000)
Kacimov, A.R.: Three-dimensional groundwater flow to a shallow pond: an explicit solution. J. Hydrol. **337**, 200–206 (2007)
Kacimov, A.R.: Analytical solution for a phreatic groundwater fall: the Riesenkampf and Numerov solutions revisited. Hydrogeol. J. **20**(6), 1203–1209 (2012). doi:10.1007/s10040-012-0857-z
Kacimov, A.R., Brown, G.: A transient phreatic surface mound, evidenced by a strip of vegetation in an earth dam shoulder: the Lembke–Youngs reductionist model revisited. Hydrol. Sci. J. **60**(2), 361–378 (2015)
Kacimov, A.R., Obnosov, Y.V.: Analytical solution to 2D problem for an anticline-diverted brine flow with a floating hydrocarbon trap. Transp. Porous Media **71**(1), 39–52 (2008). doi:10.1007/s11242-007-9110-y
Kacimov, A.R., Obnosov, Y.V., Abdalla, O., Castro-Orgaz, O.: Groundwater flow in hillslopes: analytical solutions by the theory of holomorphic functions and hydraulic theory. Appl. Math. Modell. **39**, 3380–3397 (2015). doi:10.1016/j.apm.2014.11.016
Marra, W.A., Braat, L., Baar, A.W., Kleinhans, M.G.: Valley formation by groundwater seepage, pressurized groundwater outbursts and crater-lake overflow in flume experiments with implications for Mars. Icarus **232**, 97–117 (2014)
Polubarinova-Kochina, P.Y.: Theory of Ground Water Movement. Princeton University Press, Princeton (1962). Second edition of the book in Russian, Nauka, Moscow (1977)
Press, W.H., Teukolsky, S.A., Vetterling, W.T., Flannery, B.P.: Numerical Recipes: The Art of Scientific Computing, 3rd edn. Cambridge University Press, Cambridge (2007)
Read, W.W., Volker, R.E.: Series solutions for steady seepage through hillsides with arbitrary flow boundaries. Water Resour. Res. **29**, 2871–2880 (1993)
Rushton, K.R., Youngs, E.G.: Drainage of recharge to symmetrically located downstream boundaries with special reference to seepage faces. J. Hydrol. **380**, 94–103 (2010)
Strack, O.D.L.: Groundwater Mechanics. Prentice Hall, Englewood Cliffs (1989)
Toth, J.: Gravitational Systems of Groundwater Flow-Theory, Evaluation, Utilization. Cambridge University Press, Cambridge (2009)
Townley, L.R., Trefry, M.G.: Surface water–groundwater interaction near shallow circular lakes: flow geometry in three dimensions. Water Resour. Res. **36**(4), 935–948 (2000)
Tromp-van Meerveld, H.J., Peters, N.E., McDonnell, J.J.: Effect of bedrock permeability on subsurface stormflow and the water balance of a trenched hillslope at the Panola Mountain Research Watershed, Georgia, USA. Hydrol. Process. **21**, 750–769 (2007)
Wang, S., Vafai, K., Mukhopadhyay, S.: Two-phase $CO_2$ migration in tilted aquifers in the presence of groundwater flow. Int. J. Heat Mass Transf. **77**, 717–729 (2014)
Wolfram, S.: Mathematica. A System for Doing Mathematics by Computer. Addison-Wesley, Redwood City (1991)

Youngs, E.G., Rushton, K.R.: Dupuit–Forchheimer analyses of steady-state water table heights due to accretion in drained lands overlaying undulating sloping impermeable beds. J. Irrig. Drain. Eng. ASCE **135**(4), 467–473 (2009)